NANO LETTERS

Letter

pubs.acs.org/NanoLett

Imaging the Atomic Surface Structures of CeO_2 Nanoparticles

Yuyuan Lin,*[,†] Zili Wu,[‡] Jianguo Wen,[§] Kenneth R. Poeppelmeier,*[,∥] and Laurence D. Marks*[,†]

[†]Department of Materials Science and Engineering, Northwestern University, Evanston, Illinois 60208, United States

[‡]Chemical Science Division and Center for Nanophase Materials Sciences, Oak Ridge National Laboratory, Oak Ridge, Tennessee, 37831, United States

[§]Electron Microscopy Center, Argonne National Laboratory, Argonne, Illinois 60439, United States

[∥]Department of Chemistry, Northwestern University, Evanston, Illinois 60208, United States

Supporting Information

ABSTRACT: Atomic surface structures of CeO_2 nanoparticles are under debate owing to the lack of clear experimental determination of the oxygen atom positions. In this study, with oxygen atoms clearly observed using aberration-corrected high-resolution electron microscopy, we determined the atomic structures of the (100), (110), and (111) surfaces of CeO_2 nanocubes. The predominantly exposed (100) surface has a mixture of Ce, O, and reduced CeO terminations, underscoring the complex structures of this polar surface that previously was often oversimplified. The (110) surface shows "sawtooth-like" (111) nanofacets and flat CeO_{2-x} terminations with oxygen vacancies. The (111) surface has an O termination. These findings can be extended to the surfaces of differently shaped CeO_2 nanoparticles and provide insight about face-selective catalysis.

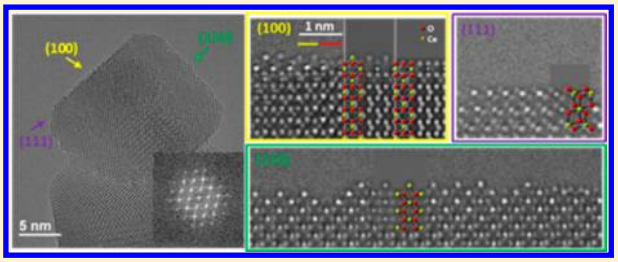

KEYWORDS: *CeO_2, atomic surface structures, aberration corrected HREM, nanocube, nanoparticle catalysis*

CeO_2 has wide applications ranging from catalysis[1−4] to solid oxide fuel cells (SOFCs).[5−7] Most of the interesting properties of CeO_2 are related to its atomic surface structures. For example, surface oxygen vacancies are expected to promote catalytic metal particle dispersion when CeO_2 is used as a catalytic support.[8,9] Under reducing conditions, O vacancies start to form on the surface, which accompanies the reduction of neighboring Ce^{4+} ions to Ce^{3+}. This reduction is believed to facilitate oxygen vacancy formation.[10] Moreover, Ce^{3+} and O vacancies can behave as the active sites for many catalytic reactions.[11−13] CeO_2 has also been explored as a SOFC anode material, where electro-catalytic activity occurs most prominently at the CeO_2/gas interface.[14]

The literature on CeO_2 surface structures is extensive. Most surface studies have focused on CeO_2 single crystals, especially the (111) surface, using scanning probe microscopy.[15−17] However, the atomic surface structures of catalytically more relevant CeO_2 nanoparticles are still not clear. High-resolution electron microscopy (HREM) is often used to study the atomic surface structures of nanoparticles.[18−20] Recently, aberration-corrected HREM studies were able to image the Ce atoms at the surface of CeO_2 nanoparticles[21−23] but not the O atoms. The conclusions of these studies appear to be contradictory for the (100) surface structures. A significant problem in the previous HREM studies was that they were unable to image the O atoms. Moreover, most of the previous surface studies were on irregularly shaped CeO_2 nanoparticles with the {111} facets predominantly exposed. Studies have shown that the (100) and (110) surfaces have superior oxygen storage capacity[24] and catalytic activity compared to the (111) surface of CeO_2.[25−27] Atomic-level characterization of the CeO_2 nanocubes (with mostly {100} facets exposed) could lead to an understanding of surface stabilization mechanisms of the high energy (100) surface as well as the structure of active sites for catalysis. In the present work, with the O atoms clearly resolved, we describe a comprehensive study on the atomic surface structures of CeO_2 nanocubes using chromatic (Cc) and spherical (Cs) aberrations corrected HREM.

The CeO_2 nanocubes were synthesized via a hydrothermal method as detailed elsewhere.[28] Figure 1 shows the general

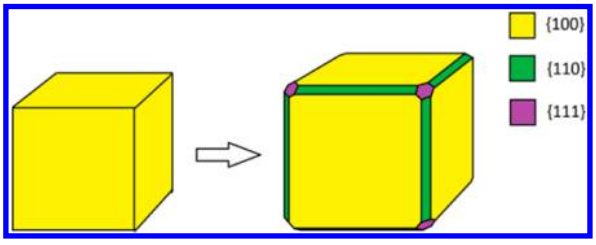

Figure 1. Exposed facets of CeO_2 nanocubes. The left one is a simplified shape and the right one is more realistic. Besides the predominantly exposed {100} facets, {110} and {111} facets exist as minor facets.

Received: October 4, 2013
Revised: November 18, 2013
Published: December 2, 2013

   dx.doi.org/10.1021/nl403713b | *Nano Lett.* 2014, 14, 191−196

shape of CeO_2 nanocubes. Although they are called "cubes", there are a small portion of {111} and {110} facets on the nanocubes. Under the [110] zone, the {111} and {110} facets are clearly observed in our experiment, as shown in Figure 2a.

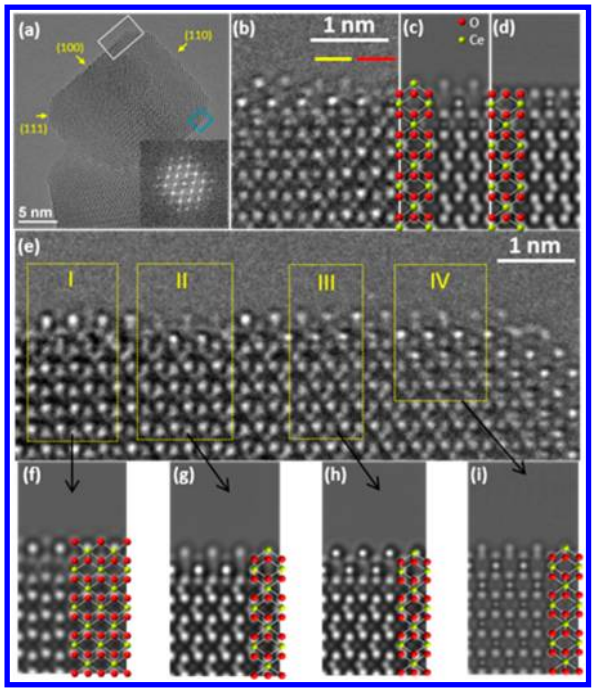

Figure 2. The {100} surfaces of CeO_2 nanocubes. (a) A HREM image on a typical CeO_2 nanocube at the [110] zone axis with the FFT of the region of interest (the area highlighted with white box) shown in the inset. (b) A magnified HREM image of the (100) surface of (a), highlighted with the blue box. (c–d) Simulated HREM images of (b) using Ce and O terminations respectively. The atomic models are directly overlaid on the atom positions of the HREM images. (e) A magnified HREM image of the (100) surface of (a), highlighted with the white box. (f) A simulated image of the region I in (e) using the $(\sqrt{2} \times \sqrt{2})R45°$ reconstructed CeO model (overlaid). (g–i) Simulated HREM images of region II, III, and IV in (e) using a Ce-terminated model.

The as-prepared nanocubes were mixed with ethanol and deposited onto a lacey carbon film supported with a copper grid. The HREM experiments were carried out using a FEI Titan 80-300 microscope operated at 200 keV with Cs and Cc corrected, using the profile imaging mode.[18−20] All the low order aberrations (up to C_5) were tuned to an acceptable level (Cs ∼ 0 μm, Cc < 1 μm, astigmatisms ∼ 0 μm) before image recording. A Cc corrector enhances resolution and localization of HREM images[29] and assists with imaging light atoms. For CeO_2, with a lattice constant of 5.4 Å the spacing between oxygen columns is 1.9 Å for the [110] zone axis. The atomic columns are well enough separated to be resolved by a typical Cs corrected microscope with subangstrom resolution.[30,31] However, a heavy element such as Ce will induce strong channeling contrast[32,33] in HREM images. Thus the interpretability is very sensitive to the sample tilt with respect to the crystal zone axis. In this study, we performed HREM image simulations[34] for the experimental images and found that the sample tilt was only approximately 1.5 mRad off from the crystal zone axis. In practice, noise from the supporting thin film can also reduce resolution and decrease oxygen contrast. In this study, we intentionally examined nanocubes not supported by a carbon film (see Figure 2a) and obtained HREM images with minimum noise. For all the experimental images shown in this study, we performed HREM image simulation (see Supporting Information) using the MacTempasX program based on the multislice method[34] and conventional nonlinear imaging[35] theory to understand the surface contrast.

Figure 2 shows the atomic surface structures of the {100} facets of a CeO_2 nanocube. Owing to the cubic shape of the particle, there are two visible {100} edges under the [110] zone axis, indicated by the white and blue boxes in Figure 2a. Figure 2b shows the HREM image of the region indicated by the blue box. Two distinctive edge-on contrasts are present in Figure 2b, as indicated by yellow and red bars. The one indicated by the yellow bar is a surface with a Ce termination with the simulated HREM image shown in Figure 2c. The red bar indicates a surface with an O termination, which matches well with the simulated HREM image with the O-terminated surface, as shown in Figure 2d. Therefore, both O and Ce terminations can exist on the same surface.

On the other (100) facet (indicated by white box in Figure 2a), a larger surface area is observable, as shown in Figure 2e. At the right part of Figure 2e (region IV), the sample is thin and the weak phase object approximation (WPOA) is approximately valid: the bright spots are atoms for a small overfocus. Thus, the surface is Ce-terminated for region IV. The simulated image of region IV is shown in Figure 2i. When the thickness is larger, the electron channeling contrast becomes dominant. Therefore, in the regions I–III of Figure 2e, the Ce columns become black spots in the bulk and the O columns are brighter than those in region IV. The exceptions are from the surface and subsurface atom columns. The bright spots of the surface and subsurface Ce columns indicate low occupancies. Figure 2f–h are the simulated HREM images for regions I–III respectively. The experimental and simulated images match reasonably well. For Figure 2f, we used the $(\sqrt{2} \times \sqrt{2})R45°$ reconstructed CeO model (half of the outermost surface O are removed in a checkerboard style,[36] the atomic model is overlaid) with the detailed surface occupancies shown in the Supporting Information. An image taken under slightly less defocus at the same area can further confirm the CeO termination (see Supporting Information). Figure 2g,h shows simulated HREM images using a Ce-terminated model with different surface atom occupancies (see Supporting Information). The simulated images from the surfaces with 100% occupancy, which are very different from the experimental contrast, are also shown in the Supporting Information. The surface spot positions in Figure 2f,g are more ordered than the ones in the experimental image. This is expected as low occupancy indicates vacancies in crystal. The disordered vacancies can result in lattice relaxation and breaks the ordered symmetry in real samples. The simulation program only treats low occupancies by lowering crystal potential and the column positions are fixed. It is worth noting that the partial occupancy of the outermost layer results in the exposure of the subsurface layer. Therefore, in terms of the exposed surface layer, it can be the CeO, Ce, or O layer.

A feature of {100} surfaces observed in this study is the hopping of atoms on the surface, which is in agreement with previous HREM studies on CeO_2 nanoparticles.[21,23] The surface atoms are diffusing on the surface (see Supporting Information), which results in random and unpredictable surface atomic rearrangements. However, similar features to Figure 2b,e are present in almost all of our HREM images.

dx.doi.org/10.1021/nl403713b | Nano Lett. 2014, 14, 191–196

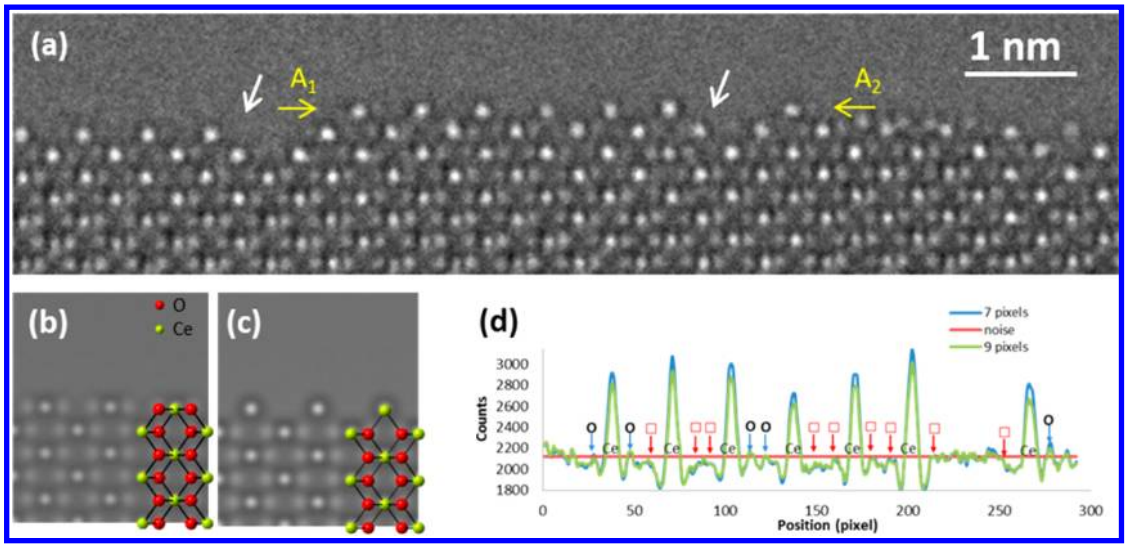

Figure 3. The (110) surfaces of CeO_2 nanocubes. (a) An experimental HREM image on a (110) surface of CeO_2 nanocubes at [110] zone axis. The white arrows indicate (111) nanofacets. (b) A simulated HREM image of the CeO_2 (110) surface with a CeO_2 surface termination. The structural model is overlaid on the atom positions. (c) A simulated HREM image of the CeO_2 (110) surface with a Ce termination. (d) Integrated line profiles from A1 to A2 indicated in (a). O vacancies are indicated by the squares (□).

Therefore, this single image represents the general features on the surface. We also reduced the electron beam intensity (from 4×10^3 to 5×10^2 e/Å^{2}s) to probe electron beam effects on the surface diffusion; however the surface hopping seems to be unavoidable. To test whether the observed surface structures are due to electron beam irradiation, we also performed infrared spectroscopy (IR) studies (see Supporting Information and ref 37). The results indicate the presence of the multiple surface structures (Ce, O, and CeO terminations) as well without the electron beam. We will return to the IR results later.

The bulk-terminated (100) surface of CeO_2 is a type-III unstable polar surface according to Tasker's polar surface notation.[38] Simplified models using an O-terminated surface with half of the outermost O atoms removed were often assumed to compensate for the dipole moment.[36,39] However, the exact surface termination is still under debate. A well-ordered $\sqrt{2}/2(3 \times 2)R45°$ surface reconstruction was observed on CeO_2 (100) single crystal using scanning tunneling microscopy.[40] When it comes to nanoparticles, Kirkland et al. used HREM with exit wave reconstruction (EWR) and concluded that the (100) surface is Ce-terminated.[22] In contrast, Möbus et al. concluded that the (100) surface of CeO_2 consists of hopping CeO chains based on their HREM and molecular dynamics simulation.[21,23]

From the present study, we conclude that the half O missing model is oversimplified. The exposed surface has mixed terminations of Ce, O, and CeO. The reconstructed region can extended to ∼1 nm deep from the outermost surface, as indicated by the partial occupancies of surface atoms in Figure S2j−m in the Supporting Information. The combination of the mixed outermost surface terminations as well as the partially occupied near-surface region is believed to quench the surface dipole moment. Mixed terminations are usually present when the energy difference among different structural configurations is small (less than 0.1 eV/1 × 1 cell). Taking entropy of mixing into account, the combination of locally ordered different structures can result in a thermodynamically stable surface (low Gibbs free energy).[41,42] Indeed, a DFT study of CeO_2 (100) has suggested that the energy difference between the different reduced surface models is quite small, and the authors suggested that deviation from a perfect atomic arrangement could easily alter the order of low energy surface configurations.[36] Our study is also in agreement with a recent XPS study on Sm-doped CeO_2 (100) surface, which showed higher Ce^{3+} concentrations near the surface than in the bulk.[43] The authors attributed the higher concentration of surface Ce^{3+} to the higher partial molar entropy of surface oxygen, suggesting the presence of different configurations in near-surface regions as well. This study shows that O vacancies are present as deep as ∼1 nm from the surface. This is consistent with a previous EELS-STEM study,[44] which shows reduced shells on the nanoparticles. As a cross-check for the surface structures, we performed IR studies of methanol adsorption on ceria nanocubes (see Supporting Information and ref 37). The multiple modes of adsorbed methanol, that is, on-top, bridging, and triply bonded methoxy species, suggest that the surfaces of CeO_2 nanocubes contain more than just one type of termination. Instead, the presence of multiple surface structures and the existence of local Ce terminations on CeO_2 nanocubes have to be invoked for the observation of a variety of methoxy species. Although {110} and {111} corners and edges are present on the CeO_2 nanocubes, the contribution of these sites to the total methoxy adsorption should be negligible (see Supporting Information). These mixed surface terminations should be intrinsic to the pristine {100} surfaces of the nanocubes.

A typical HREM image of the (110) surface is shown in Figure 3a. The surface has mixed terminations of flat CeO_{2-x} layers and "sawtooth-like" (111) nanofacets (indicated by the white arrows in Figure 3a). We investigated the HREM images of 3 different nanocubes, and found the (111) nanofacets are often ∼1 nm in length and contribute approximately 40% of the area of the {110} facets of CeO_2 nanocubes. The (110) surface of the nanocubes is very thin along the [110] direction; our simulation shows that the thickness is approximately 1.5 nm. Figure 3b shows the simulated HREM image with a CeO_2-terminated (110) surface while Figure 3c shows the one with a

dx.doi.org/10.1021/nl403713b | Nano Lett. 2014, 14, 191−196

Ce-terminated (110) surface. As the noise of Figure 3a is only from the vacuum, which is rather low, an undetectable contrast of the O column can be directly interpreted as O vacancies. Figure 3d shows the line profile of the surface layer from A1 to A2 (DigitalMicrograph, with line widths of 7 and 9 pixels). The averaged line profile intensity on the vacuum area is shown in Figure 3d, which is approximated to the noise level. Therefore, on the flat part (CeO_{2-x} part) of the CeO_2 (110) surface, there are many surface O vacancies. Using the same analysis for two other nanocubes, we found there are approximately 30% oxygen vacancies on the CeO_{2-x} part of the (110) surface. It is worth noting the ratio of the oxygen vacancies may change with oxygen vapor pressure and electron beam irradiation. Nevertheless, the ratio indicates the relative ease of oxygen vacancies formation compared to the CeO_2 (111) facet (a point we will return later) and surfaces of other oxide nanoparticles.[19,20]

Along the [110] direction, the ceria crystal consists a stack of identical neutral CeO_2 planes, which results in zero net dipole moment. However, the surface energy of the (110) surface is higher than the (111) surface.[39,45,46] The rearrangement of the surface to (111) nanofacets can reduce the high surface energy. The (111) nanofacets were observed by previous HREM studies on CeO_2 nanoparticles[47] and on a CeO_2 single crystal.[48] Moreover, the (110) surface with high concentration of O vacancies as observed in this study is in accordance with our previous IR and UV Raman studies,[28,37] in which a large amount of defect sites were observed on the ceria nanorods, which is presumably represented by {110} facets.

The (111) facet is O-terminated, based on the comparison between the experimental image and the two simulated HREM images with O-terminated and Ce-terminated surfaces, as shown in Figure 4a–c, respectively. The simulation with the O-terminated surface matches with the experimental surface contrast much better than the simulation with the Ce-terminated surface. Usually the (111) surface is classified as a type-II nonpolar surface. It is worth noting that this classification is only based on the assumption that the surface is O-terminated, as the cation layer termination will result in a type-III surface.[38] Therefore, the O termination was assumed. The previous study[22] using HREM with EWR indicates the (111) surface of CeO_2 is O-terminated as well. In this study, the surface O atoms are directly observed. The uniform surface termination of the (111) facet is consistent with the methanol probing experiment on {111} facets exposed ceria nanooctahedra where only on-top methoxy is observed.[37]

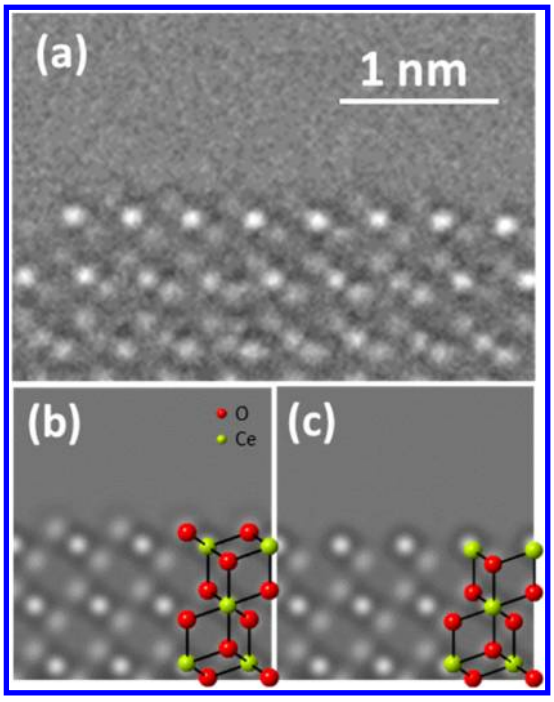

Figure 4. The (111) surfaces of CeO_2 nanocubes. (a) An experimental HREM image on a (111) surface of CeO_2 nanocubes at [110] zone axis. (b) A simulated HREM image of the CeO_2 (111) surface with an O termination. The structural model is overlaid on the atom positions. (c) A simulated HREM image of the CeO_2 (111) surface with a Ce termination.

The present results demonstrate that HREM can image both heavy and light elements simultaneously at atomic resolution. However, understanding the contrast of the atoms is not always straightforward. Ce atoms become black spots at the thick region while O atoms maintain white spots. Image simulation should be carefully conducted to understand HREM contrast. Other electron microscopy based techniques such as aberration-corrected dark field STEM (HAADF-STEM) is capable of detecting atoms[49−52] and often the contrast can be directly understood. However, HAADF-STEM has relatively low sensitivity to light elements such as O atoms when heavy elements are present.[22,44] It is worth noting bright-field STEM (BF-STEM) can image the O atoms clearly;[53] the contrast should be understood using image simulation as well, because BF-STEM and HREM have the reciprocity relationship and image contrasts are equivalent.[54] Oxide surfaces are usually more complex than surfaces of metals. Different imaging modes in electron microscopy,[18,22,55] as well as other nonelectron based techniques can all help to fully understand oxide surfaces.

In summary, we have directly observed the atomic surface structures of CeO_2 nanocubes by resolving both the O and Ce atoms with aberration-corrected HREM. The predominantly exposed (100) surface has mixed terminations with Ce, O, and CeO on the outermost surface as well as the partially occupied atoms in the near surface region. It is interesting to compare the surface stabilization mechanisms of the other materials with polar surfaces, particularly for nanomaterials, as the atomic surface structures of most oxide nanoparticles are still unclear. The (110) and (111) facets are also studied in the present work. The (110) surface has (111) nanofacets as well as CeO_{2-x} terminations. The (111) surface is ideally truncated with an O termination. Since face-selective catalysis is becoming an active research topic, these data are of particular significance when correlating the catalytic performances of nanoshapes to their corresponding exposed surface facets. The CeO_2 nanocubes ({100}-facet-dominated), nanorods ({110}-facet-dominated), and nanooctahedra ({111}-facet-dominated) often show significant differences in many catalytic reactions.[27,56−58] The results here highlight that oxide nanocrystals are not always perfectly structured, in contradiction to previous assumptions. Instead, surface reconstruction, nanofaceting, and surface vacancies have to be taken into account when constructing the structure-catalysis relationship for oxide nanomaterials.

■ ASSOCIATED CONTENT

Supporting Information

Parameters for HREM simulations, occupancies used in HREM simulations, HREM simulations with 100% occupancy of the surface atoms, an experimental HREM image with less defocus,

dx.doi.org/10.1021/nl403713b | Nano Lett. 2014, 14, 191−196

experimental time-series images show the atoms hopping on the surface, and detailed IR studies on the CeO_2 nanocrystals. This material is available free of charge via the Internet at http://pubs.acs.org.

AUTHOR INFORMATION

Corresponding Authors

*E-mail: (Y.L.) YuyuanLin2014@u.northwestern.edu.
*E-mail: (K.R.P.) krp@northwestern.edu.
*E-mail: (L.D.M.) l-marks@northwestern.edu.

Notes

The authors declare no competing financial interest.

ACKNOWLEDGMENTS

We acknowledge funding from Northwestern University Institute for Catalysis in Energy Processes (ICEP) on Grant DOE DE-FG02-03-ER15457 (Y.L., K.R.P., and L.D.M.). The electron microscopy was performed at the Electron Microscopy Center for Materials Research at Argonne National Laboratory, a U.S. Department of Energy Office of Science Laboratory operated under Contract No. DE-AC02-06CH11357 by UChicago Argonne, LLC. The synthesis of CeO_2 nanoparticles and the IR work were conducted at Oak Ridge National Laboratory and sponsored by the Division of Chemical Sciences, Geosciences, and Biosciences, Office of Basic Energy Sciences, U.S. Department of Energy. Part of the synthesis and IR work were conducted at the Center for Nanophase Materials Sciences, which is sponsored at Oak Ridge National Laboratory by the Scientific User Facilities Division, Office of Basic Energy Sciences, U.S. Department of Energy.

REFERENCES

(1) Trovarelli, A. *Catal. Rev.* **1996**, *38* (4), 439−520.
(2) Ratnasamy, C.; Wagner, J. P. *Catal. Rev.* **2009**, *51* (3), 325−440.
(3) Beckers, J.; Rothenberg, G. *Green Chem.* **2010**, *12* (6), 939−948.
(4) Vivier, L.; Duprez, D. *ChemSusChem* **2010**, *3* (6), 654−678.
(5) Mogensen, M.; Sammes, N. M.; Tompsett, G. A. *Solid State Ionics* **2000**, *129* (1−4), 63−94.
(6) Park, S.; Vohs, J. M.; Gorte, R. J. *Nature* **2000**, *404* (6775), 265−267.
(7) Atkinson, A.; Barnett, S.; Gorte, R. J.; Irvine, J. T. S.; McEvoy, A. J.; Mogensen, M.; Singhal, S. C.; Vohs, J. *Nat. Mater.* **2004**, *3* (1), 17−27.
(8) Campbell, C. T.; Peden, C. H. F. *Science* **2005**, *309* (5735), 713−714.
(9) Ta, N.; Liu, J.; Chenna, S.; Crozier, P. A.; Li, Y.; Chen, A.; Shen, W. *J. Am. Chem. Soc.* **2012**, *134* (51), 20585−20588.
(10) Skorodumova, N. V.; Simak, S. I.; Lundqvist, B. I.; Abrikosov, I. A.; Johansson, B. *Phys. Rev. Lett.* **2002**, *89* (16), 166601.
(11) Murugan, B.; Ramaswamy, A. V. *J. Am. Chem. Soc.* **2007**, *129* (11), 3062−3063.
(12) Kim, H. Y.; Lee, H. M.; Henkelman, G. *J. Am. Chem. Soc.* **2011**, *134* (3), 1560−1570.
(13) Wang, X.; Rodriguez, J. A.; Hanson, J. C.; Gamarra, D.; Martínez-Arias, A.; Fernández-García, M. *J. Phys. Chem. B* **2005**, *110* (1), 428−434.
(14) Chueh, W. C.; Hao, Y.; Jung, W.; Haile, S. M. *Nat. Mater.* **2012**, *11* (2), 155−161.
(15) Namai, Y.; Fukui, K.-i.; Iwasawa, Y. *J. Phys. Chem. B* **2003**, *107* (42), 11666−11673.
(16) Namai, Y.; Fukui, K.-I.; Iwasawa, Y. *Catal. Today* **2003**, *85* (2−4), 79−91.
(17) Esch, F.; Fabris, S.; Zhou, L.; Montini, T.; Africh, C.; Fornasiero, P.; Comelli, G.; Rosei, R. *Science* **2005**, *309* (5735), 752−755.
(18) Marks, L. D.; Smith, D. J. *Nature* **1983**, *303* (5915), 316−317.
(19) Yu, R.; Hu, L. H.; Cheng, Z. Y.; Li, Y. D.; Ye, H. Q.; Zhu, J. *Phys. Rev. Lett.* **2010**, *105* (22), 226101.
(20) Lin, Y.; Wen, J.; Hu, L.; Kennedy, R. M.; Stair, P. C.; Poeppelmeier, K. R.; Marks, L. D. *Phys. Rev. Lett.* **2013**, *111* (15), 156101.
(21) Bhatta, U. M.; Ross, I. M.; Sayle, T. X. T.; Sayle, D. C.; Parker, S. C.; Reid, D.; Seal, S.; Kumar, A.; Möbus, G. *ACS Nano* **2011**, *6* (1), 421−430.
(22) Haigh, S. J.; Young, N. P.; Sawada, H.; Takayanagi, K.; Kirkland, A. I. *ChemPhysChem* **2011**, *12* (13), 2397−2399.
(23) Möbus, G.; Saghi, Z.; Sayle, D. C.; Bhatta, U. M.; Stringfellow, A.; Sayle, T. X. T. *Adv. Funct. Mater.* **2011**, *21* (11), 1971−1976.
(24) Zhang, J.; Kumagai, H.; Yamamura, K.; Ohara, S.; Takami, S.; Morikawa, A.; Shinjoh, H.; Kaneko, K.; Adschiri, T.; Suda, A. *Nano Lett.* **2011**, *11* (2), 361−364.
(25) Mai, H.-X.; Sun, L.-D.; Zhang, Y.-W.; Si, R.; Feng, W.; Zhang, H.-P.; Liu, H.-C.; Yan, C.-H. *J. Phys. Chem. B* **2005**, *109* (51), 24380−24385.
(26) Zhou, K.; Wang, X.; Sun, X.; Peng, Q.; Li, Y. *J. Catal.* **2005**, *229* (1), 206−212.
(27) Wu, Z.; Li, M.; Overbury, S. H. *J. Catal.* **2012**, *285* (1), 61−73.
(28) Wu, Z.; Li, M.; Howe, J.; Meyer, H. M.; Overbury, S. H. *Langmuir* **2010**, *26* (21), 16595−16606.
(29) Kabius, B.; Hartel, P.; Haider, M.; Müller, H.; Uhlemann, S.; Loebau, U.; Zach, J.; Rose, H. *J. Electron Microsc.* **2009**, *58* (3), 147−155.
(30) Haider, M.; Uhlemann, S.; Schwan, E.; Rose, H.; Kabius, B.; Urban, K. *Nature* **1998**, *392* (6678), 768−769.
(31) Jia, C. L.; Lentzen, M.; Urban, K. *Science* **2003**, *299* (5608), 870−873.
(32) Howie, A. *Philos. Mag.* **1966**, *14* (128), 223−237.
(33) Van Dyck, D.; Op de Beeck, M. *Ultramicroscopy* **1996**, *64* (1−4), 99−107.
(34) Cowley, J. M.; Moodie, A. F. *Acta Crystallogr.* **1957**, *10* (10), 609−619.
(35) O'Keefe, M. A. In *Resolution-damping functions in non-linear images*, Proceedings of the 37th Annual Electron Microscopy Society of America Meeting, San Antonio, TX, 1979; Claitor's: San Antonio, TX, 1979; p 556.
(36) Skorodumova, N. V.; Baudin, M.; Hermansson, K. *Phys. Rev. B* **2004**, *69* (7), 075401.
(37) Wu, Z.; Li, M.; Mullins, D. R.; Overbury, S. H. *ACS Catal.* **2012**, *2* (11), 2224−2234.
(38) Tasker, P. W. *J. Phys. C: Solid State Phys.* **1979**, *12* (22), 4977.
(39) Nolan, M.; Grigoleit, S.; Sayle, D. C.; Parker, S. C.; Watson, G. W. *Surf. Sci.* **2005**, *576* (1−3), 217−229.
(40) Nörenberg, H.; Harding, J. H. *Surf. Sci.* **2001**, *477* (1), 17−24.
(41) Johnson, R. L.; Feidenhans'l, R.; Nielsen, M.; Grozea, D.; Marks, L. D. *Surf. Rev. Lett.* **1998**, *05* (02), 459−464.
(42) Kienzle, D. M.; Becerra-Toledo, A. E.; Marks, L. D. *Phys. Rev. Lett.* **2011**, *106* (17), 176102.
(43) Chueh, W. C.; McDaniel, A. H.; Grass, M. E.; Hao, Y.; Jabeen, N.; Liu, Z.; Haile, S. M.; McCarty, K. F.; Bluhm, H.; El Gabaly, F. *Chem. Mater.* **2012**, *24* (10), 1876−1882.
(44) Turner, S.; Lazar, S.; Freitag, B.; Egoavil, R.; Verbeeck, J.; Put, S.; Strauven, Y.; Van Tendeloo, G. *Nanoscale* **2011**, *3* (8), 3385−3390.
(45) Branda, M. a. M.; Ferullo, R. M.; Causà, M.; Illas, F. *J. Phys. Chem. C* **2011**, *115* (9), 3716−3721.
(46) Jiang, Y.; Adams, J. B.; Schilfgaarde, M. v. *J. Chem. Phys.* **2005**, *123* (6), 064701.
(47) Crozier, P. A.; Wang, R.; Sharma, R. *Ultramicroscopy* **2008**, *108* (11), 1432−1440.
(48) Nörenberg, H.; Briggs, G. A. D. *Surf. Sci.* **1999**, *433*−*435* (0), 127−130.
(49) Ohtomo, A.; Muller, D. A.; Grazul, J. L.; Hwang, H. Y. *Nature* **2002**, *419* (6905), 378−380.
(50) Suenaga, K.; Sato, Y.; Liu, Z.; Kataura, H.; Okazaki, T.; Kimoto, K.; Sawada, H.; Sasaki, T.; Omoto, K.; Tomita, T.; Kaneyama, T.; Kondo, Y. *Nat. Chem.* **2009**, *1* (5), 415−418.

(51) Shah, A. B.; Ramasse, Q. M.; Zhai, X.; Wen, J. G.; May, S. J.; Petrov, I.; Bhattacharya, A.; Abbamonte, P.; Eckstein, J. N.; Zuo, J.-M. *Adv. Mater.* **2010**, *22* (10), 1156−1160.
(52) Yankovich, A. B.; Puchala, B.; Wang, F.; Seo, J.-H.; Morgan, D.; Wang, X.; Ma, Z.; Kvit, A. V.; Voyles, P. M. *Nano Lett.* **2012**, *12* (3), 1311−1316.
(53) Hojo, H.; Mizoguchi, T.; Ohta, H.; Findlay, S. D.; Shibata, N.; Yamamoto, T.; Ikuhara, Y. *Nano Lett.* **2010**, *10* (11), 4668−4672.
(54) Cowley, J. M. *Appl. Phys. Lett.* **1969**, *15* (2), 58−59.
(55) Zhu, Y.; Inada, H.; Nakamura, K.; Wall, J. *Nat. Mater.* **2009**, *8* (10), 808−812.
(56) Wu, Z.; Schwartz, V.; Li, M.; Rondinone, A. J.; Overbury, S. H. *J. Phys. Chem. Lett.* **2012**, *3* (11), 1517−1522.
(57) Chang, S.; Li, M.; Hua, Q.; Zhang, L.; Ma, Y.; Ye, B.; Huang, W. *J. Catal.* **2012**, *293*, 195−204.
(58) Désaunay, T.; Bonura, G.; Chiodo, V.; Freni, S.; Couzinié, J. P.; Bourgon, J.; Ringuedé, A.; Labat, F.; Adamo, C.; Cassir, M. *J. Catal.* **2013**, *297*, 193−201.